JOURNAL OF GUIDANCE, CONTROL, AND DYNAMICS
Vol. 31, No. 6, November–December 2008

Entry Guidance Performance for Mars Precision Landing

C. A. Kluever*
University of Missouri—Columbia, Columbia, Missouri 65211

DOI: 10.2514/1.36950

Future Mars missions will likely require active, closed-loop entry guidance schemes to improve landing accuracy. Generally, guidance methods can be divided into two broad categories: 1) reference-path tracking schemes, and 2) predictive path-planning schemes. This paper evaluates the performance and merits of these two guidance concepts for Mars entry. The reference-path guidance is based on Apollo entry guidance, whereas a new predictive guidance technique is developed. Numerical simulations are presented for Mars entry cases involving a spacecraft modeled on the Mars Science Laboratory mission. Monte Carlo simulations with dispersions in entry flight-path angle, drag coefficient, and atmospheric density show that the root mean square of the target miss distance is 4.21 km for the reference-path guidance and 3.00 km for the predictive guidance. Furthermore, 99% of both the reference-path and predictive guidance trajectories terminate within 10 km of the target. However, simulations show that predictive guidance performance depends strongly on knowledge of the aerodynamic and density dispersions. Based on this preliminary analysis, it appears that reference-path guidance is the better option for Mars precision landing.

Introduction

TO DATE, all five successful Mars landing missions have been unguided. That is, these spacecraft did not use a closed-loop guidance method to control the entry, descent, and landing (EDL) trajectory and, consequently, the landing-error ellipse was typically on the order of hundreds of kilometers. The two Viking spacecraft (1976) were able to generate a lift-to-drag (L/D) ratio of about 0.18 during entry; the other three successful Mars landing missions, Mars Pathfinder and the Mars Exploration Rovers (MER-A and MER-B), used ballistic entry profiles (i.e., no aerodynamic lift) [1]. In all five cases, the landing footprint was largely dependent on the accuracy of the approach navigation before atmospheric entry. For example, the landing site for Mars Pathfinder was guaranteed (with 99.7% confidence) to lie within a 299×45 km ellipse [2,3]. Improvements in approach navigation reduced the 99.7% confidence landing ellipse to 70×5 km for the MER-A and MER-B missions in 2004; knowledge errors in the entry flight-path angles were both approximately ± 0.03 deg (three-sigma values) [4]. The actual landing errors for MER-A and MER-B were 10.1 and 24.6 km (downtrack), respectively, and these errors were primarily caused by variations from the atmospheric and aerodynamic models used to predict landing.

Future Mars missions will likely require more precise EDL scenarios that use active, closed-loop guidance systems. Robotic missions may target landing sites at the higher elevations of Mars, with a landing accuracy of tens of kilometers. Human exploration missions may use a two-phase landing strategy in which the crewed spacecraft must subsequently land within tens of meters from prepositioned landed assets. In both cases, the entry spacecraft will likely have a low L/D ratio between 0.06 and 0.24, which complicates the EDL strategy because these vehicles will have a low level of control authority and limited maneuverability (for comparison, the Apollo command module had a L/D ratio of 0.3). Recently, Braun and Manning [1] summarized the characteristics of the previous five successful Mars landings and defined the new challenges for future Mars landing missions, including the need for improved landing accuracy. Lockwood et al. [5] investigated various entry body configurations and the corresponding performance impact for the Mars Science Laboratory (MSL) mission, which will use an active closed-loop guidance system to provide landing accuracy on the order of 10 km.

Although further improvements in approach navigation will reduce the landing ellipse, it is clear that closed-loop entry guidance will be necessary to achieve landing accuracy on the order of ± 10 km from a designated target. Generally, guidance schemes can be divided into two broad categories: 1) reference-path tracking methods, and 2) predictive path-planning methods. In the first case, a reference trajectory is preplanned using nominal conditions and nominal models, and the guidance attempts to remove any trajectory errors during entry and eventually track the nominal path. In the second case, a new path from the current state to the desired target state is planned by onboard prediction techniques. The final guidance phase of the Apollo entry capsule used a preplanned trajectory [6], whereas the space shuttle entry guidance uses an onboard technique to adjust the drag acceleration profile to meet terminal range constraints [7]. Carman et al. [8] and Mendeck and Carman [9] investigated the use of a reference-path guidance method derived from the Apollo guidance system for a precise Mars landing (the Apollo-based technique is the current baseline guidance scheme for the MSL mission [5,9]). Tu et al. [10] developed a predictive guidance method for a Mars landing that makes onboard adjustments to the drag acceleration profile to meet trajectory and terminal range constraints. Powell [11] has developed a predictor-corrector guidance algorithm for determining roll reversals during Mars entry.

In this paper, we evaluate the performance of reference-path and predictive guidance methods for Mars EDL operations. The reference-path guidance is based on the final phase of the Apollo guidance method using the techniques presented in [6,8,9]. A new predictive guidance method is developed. Both guidance methods generate a command for banking the vehicle about the current velocity vector to modulate the lift force for trajectory control. Simulations involve trajectory control from entry interface (EI) to parachute-deployment conditions. Vehicle characteristics and boundary conditions and constraints derived from the MSL mission are used to test both guidance methods. Numerical results are presented to assess both guidance techniques.

System Models

Equations of Motion

The governing equations for a point-mass spacecraft in a Mars-centered, Cartesian inertial frame are

Presented at the AAS/AIAA Space Flight Mechanics Meeting, Galveston, Texas, 28–31 January 2008; received 1 February 2008; revision received 31 May 2008; accepted for publication 2 June 2008.

*Professor, Mechanical and Aerospace Engineering Department; KlueverC@missouri.edu. Associate Fellow AIAA.

$$\dot{\mathbf{r}} = \mathbf{v} \tag{1}$$

$$\dot{\mathbf{v}} = \mathbf{a}_g + \mathbf{a}_a \tag{2}$$

where $\mathbf{r}$ is the inertial position vector, $\mathbf{v}$ is the inertial velocity vector, $\mathbf{a}_g$ is the acceleration due to gravity, and $\mathbf{a}_a$ is the acceleration due to aerodynamic forces. Gravitational acceleration is computed by using an inverse-square model augmented with oblateness (J_2) effects; total aerodynamic acceleration is the sum of the lift acceleration ($\mathbf{a}_L$) and the drag acceleration ($\mathbf{a}_D$), and their respective magnitudes are

$$a_L = \bar{q}SC_L/m, \qquad a_D = \bar{q}SC_D/m \tag{3}$$

where C_L and C_D are the lift and drag coefficients, S is the reference area, m is the spacecraft mass, and the dynamic pressure is $\bar{q} = \rho v_{\text{rel}}^2/2$. The relative velocity, v_{rel}, is computed by subtracting the inertial velocity of the atmosphere from the inertial velocity of the vehicle (it is assumed that the atmosphere rotates with Mars). Atmospheric density ρ is computed using a piecewise-continuous exponential model [12] with discrete values for the reference densities and scale heights at altitudes of 0, 9, 36, 60, and 115 km. Altitude is computed by subtracting the equatorial radius of Mars (3394.5 km) from the magnitude of the inertial position vector.

Vehicle Models

An MSL-derived spacecraft model is used for guidance algorithm development and evaluation. Vehicle characteristics are a combination of the MSL models presented in [1,5]. MSL uses a scaled variation of the Viking 70 deg sphere-cone aeroshell, which has been employed in every Mars landing mission due to its relatively high hypersonic drag coefficient and well-known aerodynamic database. Our capsule has a reference area of $S = 12.8825$ m^2 (shell radius is 2.025 m) and an entry mass of 2200 kg. The MSL is a symmetric body with a radial center-of-gravity offset (due to ballast), which causes it to trim aerodynamically at an angle of attack of about -15 deg to produce positive lift [5]. Although the lift and drag coefficients vary slightly with the Mach number during entry, they are held constant in this analysis with $C_D = 1.450$ and $C_L = 0.348$, which results in a constant L/D of 0.24. The ballistic coefficient is

$$\beta = m/C_D S \tag{4}$$

For the model parameters used here, $\beta = 117.78$ kg/m^2.

Inertial Navigation

Guidance algorithms rely on state feedback to determine the proper commands (bank angle, in this case) required to shape the trajectory and meet desired boundary conditions. Inertial position and velocity vector estimates for the current sample time ($\mathbf{r}_k$ and $\mathbf{v}_k$) are determined using the space shuttle "Super G" algorithm [13]. The propagated position estimate at the current sample index k is

$$\mathbf{r}_k = \mathbf{r}_{k-1} + \mathbf{v}_{k-1}\Delta t + \tfrac{1}{2}\Delta\mathbf{v}_k\Delta t + \tfrac{1}{2}\mathbf{g}_{k-1}\Delta t^2 \tag{5}$$

where Δt is the sample time or update cycle of the navigation algorithm ($\Delta t = 1$ s for this analysis). Onboard inertial measurement units (IMUs) measure the sensed nongravitational (aerodynamic) accelerations in a body-fixed frame, and these accelerations are integrated over the Δt update time step to produce the sensed velocity increment vector $\Delta\mathbf{v}_k$ (transformed to the Mars-centered inertial frame). Gravitational acceleration $\mathbf{g}_k$ is updated and computed from an inverse-square gravity model augmented with oblateness (J_2) effects:

$$\mathbf{g}_k = (-\mu/r_k^2)\left[\mathbf{u}_r + 1.5J_2\left(r_M^2/r_k^2\right)[(1 - 5\sin^2\phi)\mathbf{u}_r + 2\sin\phi\mathbf{u}_z]\right] \tag{6}$$

where μ is Mars's gravitational parameter, r_M is Mars's radius, ϕ is the latitude angle computed from the propagated position vector $\mathbf{r}_k$, $\mathbf{u}_r$ is a unit vector along $\mathbf{r}_k$, and $\mathbf{u}_z$ is a unit vector along the z axis of the Mars-centered inertial frame. Inertial velocity is also propagated to the current sample index:

$$\mathbf{v}_k = \mathbf{v}_{k-1} + \Delta\mathbf{v}_k + \tfrac{1}{2}\Delta t(\mathbf{g}_{k-1} + \mathbf{g}_k) \tag{7}$$

Finally, the position vector is updated using the difference between the current and previous gravity vector estimates:

$$\mathbf{r}_k = \mathbf{r}_k + \tfrac{1}{6}\Delta t^2(\mathbf{g}_k - \mathbf{g}_{k-1}) \tag{8}$$

IMU data are modeled by corrupting the three true aerodynamic acceleration vector components with sensor noise, which is modeled by three independent zero mean Gaussian processes, each with a standard deviation of 0.05 m/s^2.

The drag acceleration, a_D, is estimated from the governing equation for the inertial velocity rate of change along the flight path:

$$a_D = -\dot{v} - \left(\mu/r_k^2\right)\sin\gamma \tag{9}$$

where γ is the current flight-path angle (computed from the $\mathbf{r}_k$ and $\mathbf{v}_k$ vectors), and the acceleration along the flight-path is approximated by the finite difference equation $\dot{v} \approx (v_k - v_{k-1})/\Delta t$. The velocity magnitude, v_k, is the norm of the inertial vector, $\mathbf{v}_k$.

Attitude Dynamics

A simple first-order, unity-gain transfer function is used to model the attitude dynamics, which are coupled with a well-tuned closed-loop attitude control system. The actual bank angle (σ) is related to the commanded bank angle (σ_c, from guidance) according to

$$\dot{\sigma} = \frac{1}{\tau}(\sigma_C - \sigma) \tag{10}$$

where $\tau = 1$ s is the time constant for the first-order lag model.

Entry Guidance Methods

The guidance problem is to determine the bank command such that the vehicle reaches the desired parachute-deployment target and meets terminal state constraints. Dynamic pressure at parachute deployment is limited to $220 \le \bar{q} \le 880$ N/m^2, and the deployment Mach number is limited to $1.2 \le M \le 2.2$.

The advantages of reference-path tracking guidance include its simplicity and ease of implementation. A drawback of reference-path guidance is that it is based on linearization methods and primarily designed for neighboring trajectories with relatively small state perturbations. Furthermore, a guidance method that solely relies on a fixed reference path may not be able to successfully control the trajectory in the presence of large aerodynamic or density variations with respect to the nominal reference values.

The advantages of predictive guidance include the potential to dramatically reduce terminal errors and/or reshape the trajectory in the presence of significant state, vehicle, and atmospheric dispersions. A drawback of predictive guidance is that it usually relies on accurate aerodynamic and atmospheric models to predict the future terminal states.

Reference-Path Tracking Guidance

Carman et al. [8] developed a reference-path guidance method for the Mars Surveyor Program lander mission, which was designed for launch in 2001. The final phase of the Apollo entry guidance scheme (after the skip-out phase) was adapted and modified for the entry phase of this Mars mission, and it has subsequently been adapted for the MSL mission [5,9]. The reference-path tracking guidance developed for this paper is also based on the Apollo guidance and the methods presented in [8,9]. An overview of this guidance method is presented; details can be found in [6,8,9].

The commanded vertical L/D component λ_C is computed from linear perturbation theory and the stored reference trajectory:

$$\lambda_C = \lambda_{\text{ref}} + K_3 \frac{\partial(L/D)}{\partial R}(R_{\text{go}} - R_{\text{pred}}) \tag{11}$$

where λ_{ref} is the reference vertical L/D component, and R_{go} is the actual range to go computed using the current position vector of the vehicle and the position vector of the targeted site (parachute deployment). The Mars-rotation effect on the target's position vector is included by using an estimate for the remaining flight time. Predicted range to go (R_{pred}) is a function of the stored reference range to go (R_{ref}) and the altitude rate ($\dot{r}$) and drag errors:

$$R_{\text{pred}} = R_{\text{ref}} + \frac{\partial R}{\partial \dot{r}}(\dot{r} - \dot{r}_{\text{ref}}) + \frac{\partial R}{\partial a_D}(a_D - a_{D\text{ref}}) \tag{12}$$

All reference values are computed by interpolating the stored reference profile with energy E as the independent variable, that is,

$$R_{\text{ref}} = f_1(E), \qquad \dot{r}_{\text{ref}} = f_2(E), \qquad a_{D\text{ref}} = f_3(E) \tag{13}$$

where $E = v^2/2 - \mu/r$. Energy is used here instead of velocity, because velocity is not monotonic due to the steep flight-path angle at atmospheric entry (Carman et al. [8] and Mendeck and Carman [9] used velocity as the independent variable).

The partial derivatives in Eqs. (11) and (12) are essentially feedback gains, and they are computed using the method of adjoints and backward integration of the linearized system in the same manner as [8]. Gain $K_3 = 4$ is an "overcontrol gain, " which amplifies all feedback errors to speed up the transient response. Therefore, the closed-loop guidance law (11) has the general form

$$\lambda_C = \lambda_{\text{ref}} + K_R(R_{\text{go}} - R_{\text{ref}}) + K_{RD}(\dot{r} - \dot{r}_{\text{ref}}) + K_d(a_D - a_{D\text{ref}}) \tag{14}$$

The feedback gains (which are combinations of the adjoint variables) are stored as a function of energy:

$$K_R(E) = K_3 \frac{\partial(L/D)}{\partial R} \tag{15}$$

$$K_{RD}(E) = -K_3 \frac{\partial(L/D)}{\partial R}\frac{\partial R}{\partial \dot{r}} \tag{16}$$

$$K_d(E) = -K_3 \frac{\partial(L/D)}{\partial R}\frac{\partial R}{\partial a_D} \tag{17}$$

The bank-angle command is

$$\sigma_C = \cos^{-1}\left(\frac{\lambda_C}{L/D}\right) \tag{18}$$

where $L/D = 0.24$. The lateral guidance logic used here commands bank reversals if the crossrange error exceeds a dead-zone value, in which the dead-zone threshold is proportional to v^2 to limit the number of reversals. In particular, the crossrange threshold is approximately 3 km at EI ($v = 6$ km/s) and decreases to about 0.5 km at the velocity corresponding to parachute deployment. Bank reversals are prohibited when the relative velocity is lower than 900 m/s. Minimum and maximum bank magnitudes are set at 15 and 165 deg, respectively, and are used to impart some lateral control authority even if full lift up ($\sigma_C = 0$ deg) or full lift down ($\sigma_C = 180$ deg) is commanded.

Predictive Guidance

A new predictive guidance method is developed for tracking a reference altitude profile, which is defined by a polynomial in range to go. A fourth-order polynomial is used because it has enough flexibility to accommodate either a monotonically decreasing altitude profile or an altitude profile with both negative and positive rates of change. Furthermore, a fourth-order altitude reference can be defined by knowledge of the altitude and flight-path angle at both ends of the trajectory and the altitude at $R_{\text{go}}/2$. The reference altitude profile to parachute deployment is

$$h_{\text{ref}} = a_0 + a_1 R_{\text{go}} + a_2 R_{\text{go}}^2 + a_3 R_{\text{go}}^3 + a_4 R_{\text{go}}^4 \tag{19}$$

Note that, because $\dot{h} = v\sin\gamma$ and $\dot{R}_{\text{go}} = -(r_M/r)v\cos\gamma \approx -v\cos\gamma$ (the time rate of R_{go} is negative because the range to go is decreasing), the derivative of altitude with respect to range is the tangent of the flight-path angle:

$$\frac{\mathrm{d}h_{\text{ref}}}{\mathrm{d}R_{\text{go}}} = -\tan\gamma_{\text{ref}} = a_1 + 2a_2 R_{\text{go}} + 3a_3 R_{\text{go}}^2 + 4a_4 R_{\text{go}}^3 = h'_{\text{ref}} \tag{20}$$

where the prime indicates a derivative with respect to range. Quartic polynomial coefficients are computed from Eqs. (19) and (20) given the vehicle's current altitude and flight-path angle at the current range to go R_{go}, altitude at $R_{\text{go}}/2$, and altitude and flight-path angle at the desired parachute-deployment state ($R_{\text{go}} = 0$).

An open-loop or reference vertical L/D command can be computed directly from the reference altitude and flight-path angle profiles. To begin, we take the time derivative of $-\tan\gamma_{\text{ref}}$ to obtain

$$\frac{\mathrm{d}}{\mathrm{d}t}(-\tan\gamma_{\text{ref}}) = -(1 + \tan^2\gamma_{\text{ref}})\frac{\mathrm{d}\gamma}{\mathrm{d}t} \tag{21}$$

Using the chain rule to take the time derivative of Eq. (21) yields

$$\begin{aligned}\frac{\mathrm{d}}{\mathrm{d}t}(-\tan\gamma_{\text{ref}}) &= \frac{\mathrm{d}}{\mathrm{d}R_{\text{go}}}(-\tan\gamma_{\text{ref}})\frac{\mathrm{d}R_{\text{go}}}{\mathrm{d}t} \\ &= (2a_2 + 6a_3 R_{\text{go}} + 12a_4 R_{\text{go}}^2)\frac{\mathrm{d}R_{\text{go}}}{\mathrm{d}t} = -h''_{\text{ref}} v\cos\gamma_{\text{ref}}\end{aligned} \tag{22}$$

The dynamical equation for the flight-path angle is

$$\dot{\gamma} = \frac{a_L\cos\sigma}{v} - \frac{g\cos\gamma}{v} + \frac{v\cos\gamma}{r} \tag{23}$$

Substituting Eq. (23) into Eq. (21) and equating the result to Eq. (22) yields

$$a_L\cos\sigma = \cos\gamma_{\text{ref}}\left(g - (v^2/r) + h''_{\text{ref}} v^2\cos^2\gamma_{\text{ref}}\right) \tag{24}$$

Finally, divide Eq. (24) by drag acceleration a_D:

$$\frac{L}{D}\cos\sigma = \lambda_{\text{ref}} = \frac{\cos\gamma_{\text{ref}}}{a_D}\left(g - (v^2/r) + h''_{\text{ref}} v^2\cos^2\gamma_{\text{ref}}\right) \tag{25}$$

Local gravitational acceleration is $g = \mu/r^2$. Equation (25) is the guidance law for following a prescribed altitude reference, $h_{\text{ref}} = f(R_{\text{go}})$.

The basic idea of the proposed predictive guidance method is to select a reference altitude, $h_{\text{ref}} = f(R_{\text{go}})$, and determine the vehicle's velocity at $R_{\text{go}} = 0$ (i.e., parachute deployment). Adjustments are made to h_{ref} until the relative velocity at $R_{\text{go}} = 0$ is 400 m/s, which is the nominal trigger for parachute deployment. Therefore, the predictive guidance method requires propagating the vehicle's velocity to the terminal condition. To do this, observe the time derivative of energy:

$$\dot{E} = \frac{\mathrm{d}}{\mathrm{d}t}\left(\frac{v^2}{2} - \frac{\mu}{r}\right) = v\dot{v} + \frac{\mu}{r^2}\dot{r} \tag{26}$$

Substituting the dynamical equation for velocity along the flight path [see Eq. (9)] and the kinematic equation for altitude rate $\dot{r} = v\sin\gamma$ yields

$$\dot{E} = -a_D v \tag{27}$$

It is advantageous to propagate energy using range to go as the independent variable because it has a known final value of $R_{\text{go}} = 0$ at

parachute deployment. Therefore, dividing Eq. (27) by $\dot{R}_{\text{go}} = -v\cos\gamma$ yields

$$\frac{\mathrm{d}E}{\mathrm{d}R_{\text{go}}} = E' = \frac{a_D}{\cos\gamma_{\text{ref}}} \tag{28}$$

Note that, because both energy and range to go are monotonically decreasing, $\mathrm{d}E/\mathrm{d}R_{\text{go}}$ is positive.

The predictive guidance method can now be summarized. The energy equation (28) is propagated numerically from the current energy to the desired target (parachute deployment) using the known range to go. The reference flight-path angle is determined by the derivative of the quartic polynomial for h_{ref} [see Eq. (20)]; drag acceleration is determined from the aerodynamic force model (3), which requires knowledge of the drag coefficient C_D and an atmospheric model for density. Relative velocity at $R_{\text{go}} = 0$ (parachute deployment) is computed from the terminal inertial velocity (derived from energy and altitude), the target latitude and heading angle, and the law of cosines. To compute the five quartic polynomial coefficients for h_{ref}, the five states, $h(R_{\text{go}})$, $\gamma(R_{\text{go}})$, h_{mid}, h_f, and γ_f, must be determined. The two states at the current range to go are known, and terminal flight-path angle γ_f is fixed at the nominal value of -19 deg. The final altitude at parachute deployment is determined by scaling a nominal final altitude:

$$h_f = G_\rho G_D h_f^* \tag{29}$$

where $h_f^* = 8.5$ km is the nominal final altitude, and G_ρ and G_D are multiplicative factors that scale nominal values for the atmospheric density and drag coefficient, respectively. When the atmospheric density and/or drag coefficient is higher than nominal, the decelerating capsule will reach the 400 m/s velocity trigger at a higher altitude; the converse is true for below-nominal drag conditions. The final altitude h_f is bounded by a lower limit of 6.5 km (the parachute trigger altitude) for extreme low-drag cases. Note that for extreme high-drag cases (e.g., $G_\rho = 1.4$ and $G_D = 1.3$) the final altitude is 15.5 km. The product $G_\rho G_D$ is actually the scaling factor between the actual and nominal (model) drag forces. It was found that adjusting h_f in this manner produced a feasible quartic reference altitude at which the control did not saturate.

The reference altitude profile is updated by adjusting the midpoint altitude (at $R_{\text{go}}/2$) using the relative velocity error from the trajectory propagation step:

$$h_{\text{mid}}^{i+1} = h_{\text{mid}}^{i}(1 + 0.75\delta v_{\text{rel}}^{i}) \tag{30}$$

where h_{mid}^{i} is the midpoint altitude (in kilometers) for the ith iteration, and $\delta v_{\text{rel}}^{i} = 0.4 - v_{\text{rel}}(R_{\text{go}} = 0)$ is the terminal relative velocity error (in kilometers per second) for the ith iteration. The propagation process is repeated for a fixed number of iterations; numerical experience has shown that the terminal relative velocity converges to 400 m/s in at most 3 iterations. A simple first-order Euler integration scheme with 500 fixed steps is used to numerically propagate the energy equation (28).

Once the proper quartic reference altitude is determined, a closed-loop control law is used to track h_{ref}:

$$\lambda_C = \lambda_{\text{ref}} + K_H(h_{\text{ref}} - h) + K_{HD}(\dot{h}_{\text{ref}} - \dot{h}) \tag{31}$$

where λ_{ref} is computed using Eq. (25), and the gain K_{HD} is the same as the altitude rate gain computed using the adjoint method [see Eq. (16) with a sign change]. The altitude gain K_H is one-fifth of the gain K_{HD} to maintain a 5:1 ratio between the rate and proportional gains. Finally, it should be noted that the altitude reference is updated every 20 s using the propagation method and Eq. (30), and that the predictive guidance uses the lateral bank-reversal logic described in the previous subsection.

Numerical Results

Several Mars entry trajectories are computed to compare and evaluate the guidance methods. Simulink is used to numerically integrate a nondimensional form of the governing point-mass equations of motion (1) and (2) and the bank dynamics (10). A third-order, Bogacki–Shampine routine is employed with a fixed step size of 0.2 s. The nominal initial conditions at EI are based on MSL data from [1]: the inertial velocity is 6 km/s, the inertial flight-path angle is -14.5 deg, and the altitude is 126 km. No initial heading error is assumed for the great circle connecting the EI and target position vectors. The simulation is terminated at parachute deployment, which is triggered when either 1) relative velocity decreases to 400 m/s, or 2) altitude decreases to 6.5 km (the v_{rel} threshold is the nominal trigger).

Before closed-loop simulation trials can be performed, the reference path must be determined. The reference trajectory was determined by running a series of open-loop entry simulations with a fixed bank angle. It is desirable that the reference trajectory be in the "middle" of the downtrack maneuvering capability of the vehicle so that the closed-loop guidance can compensate for both positive and negative range-to-go errors. Figure 1 shows the parachute-deployment footprint for several open-loop fixed bank trials with nominal initial conditions at EI. The origin of the downtrack axis is centered in the middle of the footprint, which corresponds to a fixed bank angle of 46.2 deg. Figure 1 shows that the full lift up ($\sigma = 0$ deg) and full lift down ($\sigma = 180$ deg) cases are able to extend and reduce, respectively, the downtrack range by

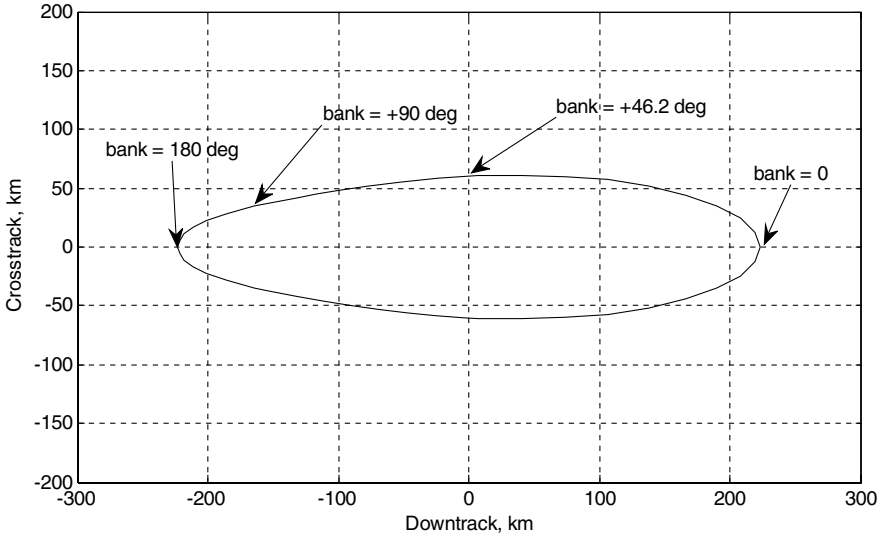

Fig. 1 Parachute-deployment footprint for open-loop entry with fixed bank angle.

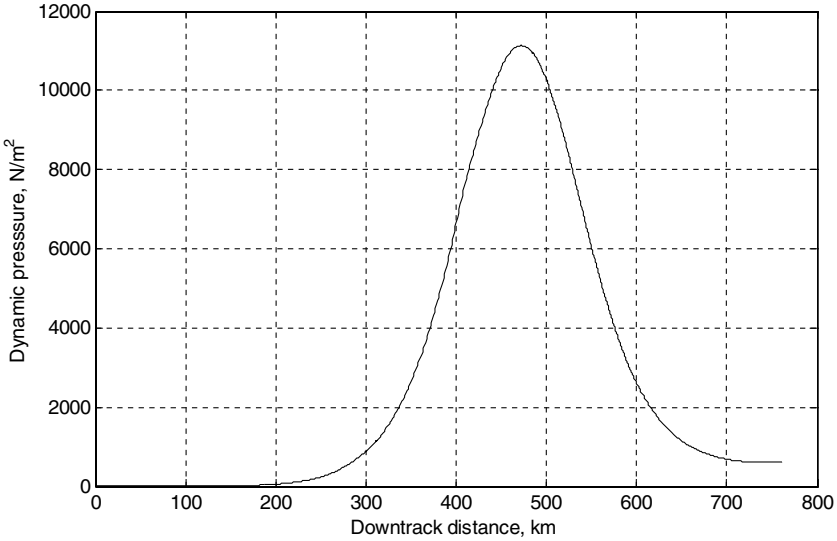

Fig. 2 Dynamic pressure for nominal entry using reference-path guidance.

approximately 220 km when compared with the reference trajectory using $\sigma = 46.2$ deg. Furthermore, Fig. 1 shows that a 46.2 deg bank provides near-maximum crossrange capability. It is interesting to note that directing all of the lift force to the side ($\sigma = 90$ deg) does not maximize the crossrange distance because the lack of a vertical lift component reduces the downtrack distance and flight time. Therefore, the reference vertical L/D component in Eq. (11) or Eq. (14) is $\lambda_{\text{ref}} = (L/D)\cos\sigma_{\text{ref}}$, where $\sigma_{\text{ref}} = 46.2$ deg.

Reference-Path Guidance: Results

Figures 2–4 present the dynamic pressure, altitude, and energy profiles vs downtrack distance for a nominal entry using the reference-path tracking guidance method. Figures 2 and 4 show that aerodynamic forces are negligible for the first one-quarter of the downtrack distance and, as a result, the energy remains nearly constant. The peak dynamic pressure occurs at an altitude and velocity of about 27 km and 4.5 km/s, respectively.

Figure 5 presents the time history of the navigation position-vector errors for a nominal entry. The figure clearly shows how position errors accumulate over time due to the integrated IMU noise. Table 1 presents the downtrack, crosstrack, and range-to-target errors at parachute deployment for this nominal case. The navigated targeting errors are slightly better than the actual errors at parachute deployment, which is to be expected because guidance uses the navigated state vector for feedback. The results from this single trajectory are representative of the expected navigation errors for all trials. Figure 5 and Table 1 show that position errors are on the order of tens of meters, which indicates that navigation errors do not have a large effect on targeting accuracy.

A 500-run Monte Carlo study was performed using the reference-path guidance method. Dispersions were considered for the atmospheric entry flight-path angle, drag coefficient, and

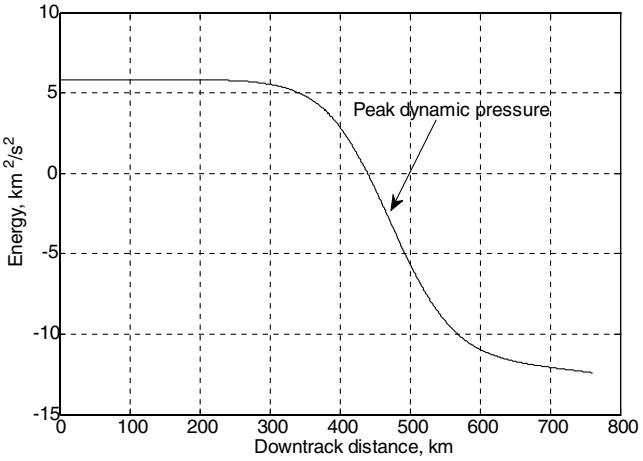

Fig. 4 Energy profile for nominal entry using reference-path guidance.

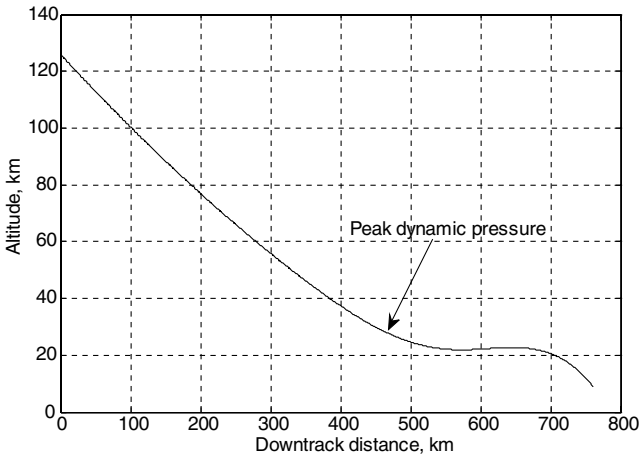

Fig. 3 Altitude profile for nominal entry using reference-path guidance.

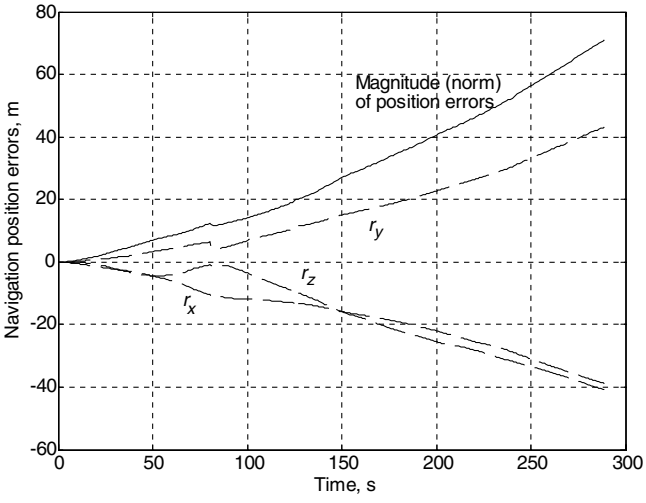

Fig. 5 Navigation position errors for nominal entry using reference-path guidance.

Table 1 Actual and navigated targeting errors for reference-path guidance

Case	Downtrack error, m	Crosstrack error, m	Range-to-target error, m
True state	−706.4	825.5	1086.5
Navigated state	−675.3	782.6	1033.7

atmospheric density; these dispersions were modeled by three independent random variables with zero means and Gaussian distributions. The initial flight-path angle dispersion is ±0.34 deg (3 standard deviations), which is consistent with the MSL analysis in [5]. The drag coefficient and density dispersions were modeled as random multiplier factors (G_D and G_ρ), each held constant over the entire entry. The drag coefficient dispersion is ±30%, or $G_D = [0.7, 1.3]$, whereas the density dispersion is ±40%, or $G_\rho = [0.6, 1.4]$. Each dispersion boundary represents 3 standard deviations from nominal.

Figure 6 shows the target miss distances at parachute deployment (end of the simulation) for the 500-run study. Each small circle represents a single entry simulation using the reference-path guidance method, and the 10 km and 5 km error boundaries are clearly labeled. In this 500-run study, 370 (or 74.0%) are within 5 km of the target, whereas 495 (or 99.0%) are within 10 km of the target. The largest miss distance from the 500 simulations is 20.25 km (not shown in Fig. 5). The rms of all target miss distances is 4.21 km. Figure 6 also shows what appears to be a correlation between downtrack and crosstrack errors, wherein trajectories that fall short of the target exhibit large positive crosstrack errors, whereas trajectories that overshoot the target exhibit large negative crosstrack errors. This phenomenon may be a consequence of the selected dead-zone corridor for bank reversals or the gain-tuning procedure.

Figure 7 presents a histogram of the terminal altitude at parachute deployment. Note that, in a significant number of the trials, parachute deployment is triggered by the minimum altitude constraint ($h \leq 6.5$ km), in which case the relative velocity is greater than 400 m/s. All 500 trials are feasible in terms of the terminal dynamic pressure and Mach constraints; the minimum and maximum values of $\bar{q}$ are 439 and 833 N/m^2, respectively, and the minimum and maximum Mach numbers are 1.63 and 2.06, respectively.

Predictive Guidance: Results

Next, a 500-run Monte Carlo study was performed using the predictive guidance method with the same dispersion characteristics.

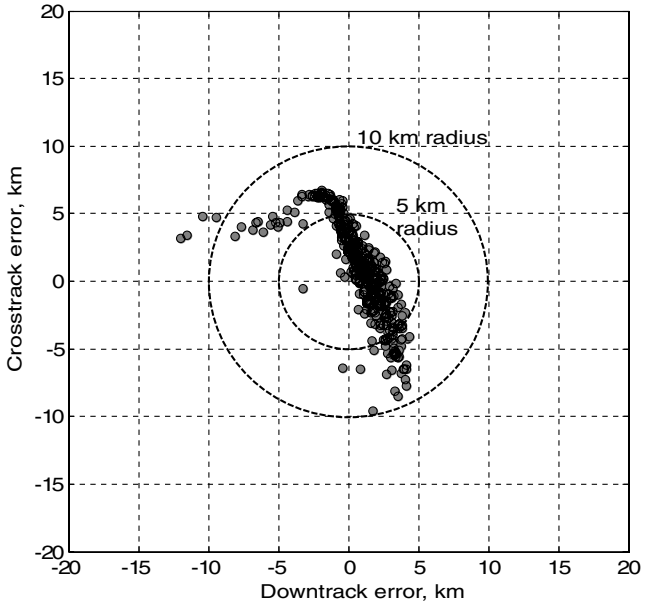

Fig. 6 Targeting errors using reference-path guidance.

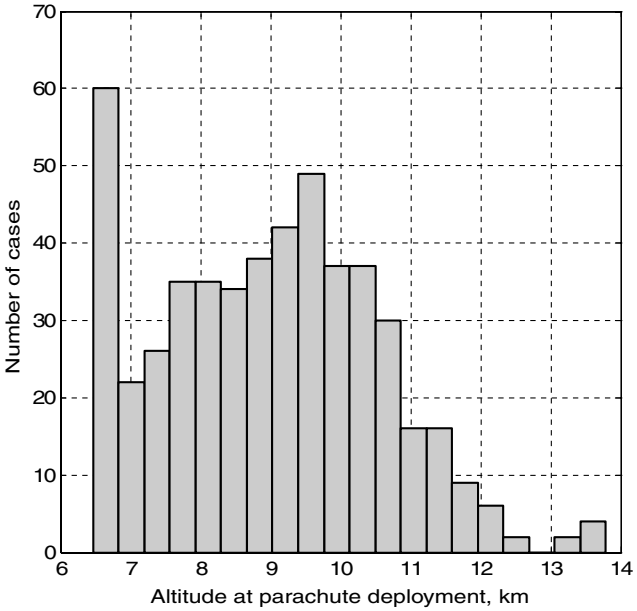

Fig. 7 Terminal altitude using reference-path guidance.

It is important to note that we assumed that the predictive guidance had exact knowledge of both the C_D and density dispersions (recall that the predictive guidance must predict and propagate drag as it updates the reference altitude in an attempt to meet terminal velocity conditions). The assumption of exact knowledge of the density and drag dispersions is unrealistic, but it will result in the best possible performance of the proposed predictive guidance. Methods for onboard estimation of drag coefficient and atmospheric density models are subjects for future research. Figure 8 shows the target miss distances at parachute deployment: 472 (or 94.4%) are within 5 km of the target, whereas 497 (or 99.4%) are within 10 km of the target. The largest miss distance from the 500 simulations is 14.60 km, and the rms of all target miss distances is 3.00 km. Therefore, the new predictive guidance method demonstrates better targeting accuracy compared with the reference-path guidance method. Note that the crosstrack errors in Fig. 8 are generally larger than the downtrack errors; an improved predictive guidance method might include the lateral dynamics to predict optimal bank reversals.

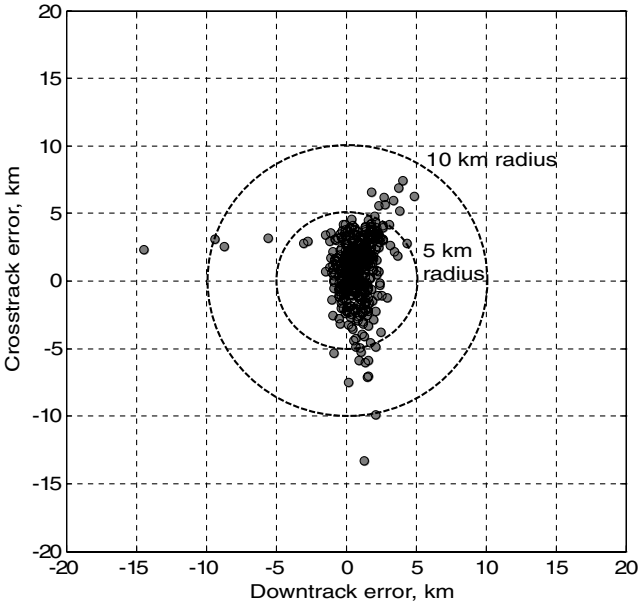

Fig. 8 Targeting errors: predictive guidance with dispersion knowledge.

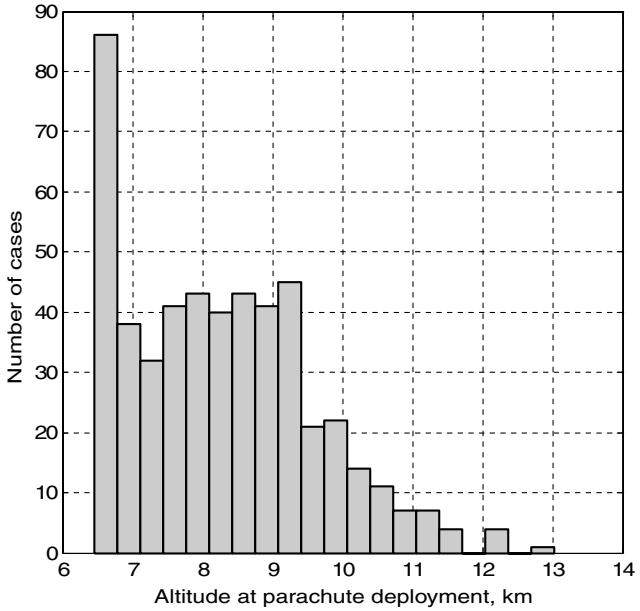

Fig. 9 Terminal altitude: predictive guidance with dispersion knowledge.

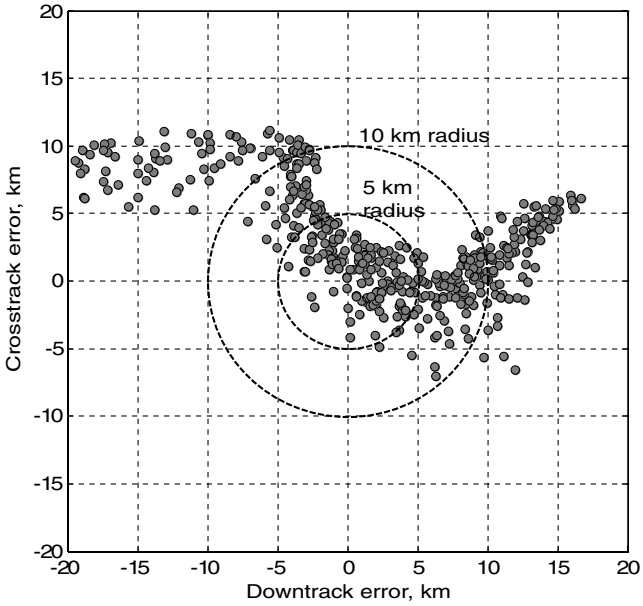

Fig. 10 Targeting errors: predictive guidance without dispersion knowledge.

Figure 9 presents a histogram of the terminal altitude at parachute deployment. A majority of terminal altitudes are near the 6.5 km altitude trigger. However, parachute deployment is actually triggered by $v_{\text{rel}} \leq 400$ m/s in 447/500 trials (89%), whereas 53/500 (11%) trials are triggered by $h \leq 6.5$ km (in two cases the terminal triggers occur simultaneously). The 6.5 km altitude trigger results from cases with low atmospheric density and/or a low drag coefficient [see Eq. (29)]. All 500 trials are feasible in terms of the terminal dynamic pressure and Mach constraints; the minimum and maximum values of $\bar{q}$ are 459 and 849 N/m^2, respectively, and the minimum and maximum Mach numbers are 1.66 and 2.11, respectively.

It should be noted that the predictive guidance will never result in zero target miss distances (even with perfect models) because the lateral dynamics and vehicle attitude dynamics are not included in the onboard guidance equations for predicting the parachute-deployment state. Therefore, the inevitable bank reversals and time lag for bank maneuvers will result in trajectories that do not exactly match the guidance propagation of the single energy equation (28). Nevertheless, the predictive guidance produces target miss distances of less than 1 km for many cases that involve relatively small dispersions. At the other extreme, the worst combination of dispersions (+40% density dispersion, +30% drag coefficient dispersion) cannot be rectified with any bank-angle program. For this worst-case drag scenario, a capsule with full lift up throughout the entry falls 17 km short of the target.

Finally, we conducted a 500-run Monte Carlo study in which the predictive guidance did not have any knowledge of either the C_D or density dispersions (only the nominal values were used by the guidance). Figure 10 shows the target miss distances at parachute deployment: 27% are within 5 km of the target, whereas 56% are within 10 km of the target. The largest miss distance from the 500 simulations is 65.50 km, and the rms of all target miss distances is 16.17 km.

Conclusions

Mars entry trajectories have been simulated using two guidance methods; the first method attempts to track a preplanned reference profile, whereas the second guidance method replans the trajectory to predict the terminal states. The reference-path guidance is derived from the final phase of the Apollo guidance scheme, and a new guidance method using an adjustable altitude profile has been developed for the predictive guidance technique. Numerical simulations have been presented for a case study based on the Mars Science Laboratory vehicle and its mission characteristics. The simulations include the effects of inertial navigation and attitude actuation. Entry trajectories terminate with a parachute deployment that is triggered by either the relative velocity or altitude, and dynamic pressure and Mach constraints are imposed at parachute deployment.

A 500-run Monte Carlo study was performed for each guidance method, with random dispersions in the entry flight-path angle, drag coefficient, and atmospheric density. A major assumption of this study is that the predictive guidance has perfect knowledge of the aerodynamic and density dispersions (the predictive guidance requires vehicle and density models to numerically propagate the energy over the range to go). The rms of the target miss distances was 4.21 km for the reference-path guidance and 3.00 km for the predictive guidance. Both the reference-path and predictive guidance trials showed that 99% of the 500 runs were within 10 km of the target. All 500 runs satisfied the terminal constraints for dynamic pressure and Mach number for both guidance methods. A separate 500-run Monte Carlo study showed that knowledge of aerodynamic and density dispersions is critical for achieving good target accuracy with the predictive guidance method. Furthermore, only 56% of the runs were within 10 km of the target when predictive guidance relied on static (nominal) aerodynamic and density models. In addition, the rms of the target miss distances increased to 16.17 km when the predictive guidance had no dispersion knowledge. Navigation errors and dispersions in the entry flight-path angle were both found to have very little effect on targeting accuracy for either guidance method.

This preliminary analysis shows that, although the predictive guidance delivers more accurate terminal conditions compared with the reference-path guidance, it relies heavily on accurate onboard models of the vehicle and the Martian atmosphere. The results presented here demonstrate the best possible performance of the proposed predictive guidance method, because exact modeling is unrealistic and any onboard estimation scheme will incur errors. Therefore, the reference-path guidance is likely the best option for a Mars precision landing. Furthermore, unlike predictive guidance, reference-path guidance does not require onboard models of the vehicle and atmosphere, which also makes it a more attractive guidance option.

References

[1] Braun, R. D., and Manning, R. M., "Mars Exploration Entry, Descent and Landing Challenges," Institute of Electrical and Electronics Engineers Paper IEEEAC 0076, Dec. 2005. doi:10.1109/AERO.2006.1655790

[2] Vaughan, R. M., Kallemeyn, P. H., and Spencer, D. A., "Navigation Flight Operations for Mars Pathfinder," American Astronautical Society Paper 98-145, Feb. 1998.

[3] Spencer, D. A., and Braun, R. D., "Mars Pathfinder Atmospheric Entry: Trajectory Design and Dispersion Analysis," *Journal of Spacecraft and Rockets*, Vol. 33, No. 5, 1996, pp. 670–676. doi:10.2514/3.26819

[4] D'Amario, L. A., "Mars Exploration Rovers Navigation Results," AIAA Paper 2004-4980, Aug. 2004.

[5] Lockwood, M. K., Powell, R. W., Sutton, K., Prabhu, R. K., Graves, C. A., Epp, C. D., and Carman, G. L., "Entry Configurations and Performance Comparisons for the Mars Smart Lander," *Journal of Spacecraft and Rockets*, Vol. 43, No. 2, 2006, pp. 258–269. doi:10.2514/1.20678

[6] Morth, R., "Reentry Guidance for Apollo," Massachusetts Inst. of Technology Instrumentation Lab., Rept. R-532, Vols. 1–2, Cambridge, MA, Jan. 1966.

[7] Harpold, J. C., and Graves, C. A., "Shuttle Entry Guidance," *Journal of the Astronautical Sciences*, Vol. 27, No. 3, 1979, pp. 239–268.

[8] Carman, G. L., Ives, D. G., and Geller, D. K., "Apollo-Derived Mars Precision Lander Guidance," AIAA Paper 98-4570, Aug. 1998.

[9] Mendeck, G. F., and Carman, G. L., "Guidance Design for Mars Smart Landers Using the Entry Terminal Point Controller," AIAA Paper 2002-4502, Aug. 2002.

[10] Tu, K.-Y., Munir, M. S., Mease, K. D., and Bayard, D. S., "Drag-Based Predictive Tracking Guidance for Mars Precision Landing," *Journal of Guidance, Control, and Dynamics*, Vol. 23, No. 4, 2000, pp. 620–628.

[11] Powell, R. W., "Numerical Roll Reversal Predictor Corrector Aerocapture and Precision Landing Guidance Algorithms for the Mars Surveyor Program 2001 Missions," AIAA Paper 98-4574, Aug. 1998.

[12] Lyne, J. E., "Physiologically Constrained Aerocapture for Manned Mars Missions," NASA TM-103954, Aug. 1992.

[13] McHenry, R. L., Brand, T. J., Long, A. D., Cockrell, B. F., and Thibodeau, J. R., "Space Shuttle Ascent Guidance, Navigation, and Control," *Journal of the Astronautical Sciences*, Vol. 27, No. 1, 1979, pp. 1–38.